Theory of reorientational transitions in ferrielectric liquid crystals

V. L. Lorman, A. A. Bulbitch, and P. Toledano
Laboratory of Phase Transitions, University of Amiens, 33 rue Saint Leu, 80039 Amiens Cedex, France
(Received 16 August 1993)

A phenomenological model is proposed for the description of the sequences of ferroelectric, antiferroelectric, and ferrielectric smectic phases reported in liquid crystals of the MHPOBC [4-(1-methylheptyloxycarbonyl)phenyl-4′-octyloxybiphenyl-4-carboxylate] type. The model assumes a bilayer smectic ordering and a mechanism consisting of an azimuthal reorientation of the molecules at the transitions. Three helicoïdal ferrielectric structures are found to be possibly stable, in which the helical pitch is shown to vary monotonically as a function of temperature. One of these phases, characterized by an azimuthal mode independent from the z coordinate, provides a suitable interpretation of the presently known results on ferrielectric ordering in liquid crystals. The static and dynamical features of the transitions are worked out and discussed in view of the available data.

PACS number(s): 64.70.Md, 61.30.Cz

I. INTRODUCTION

Since the first antiferroelectric liquid-crystalline phase was discovered in MHPOBC [4-(1-methylheptyloxycarbonyl) phenyl - 4′ - octyloxybisphenyl - 4 - carboxylate] [1], a number of antiferroelectric and ferrielectric liquid crystals have been found [2–7], such as TFMHPOBC, TFFMPOBC, TFMHPDOPB, MHPOCBC, and MOPBIC, which display a variety of sequences of different dipolar orders. In addition to the standard ferroelectric Sm-C^* phase, at least four types of new dipolar mesophases have been evidenced: the antiferroelectric Sm-C_A^* [8], the ferrielectric Sm-C_γ^* phase [9], and other phases denoted Sm-C_α^* and Sm-C_x^* [2,10]. Although an extensive set of experimental studies was performed on the preceding compounds, including x-ray diffraction [11,12], differential-scanning calorimetry [2,13,14], dielectric and optical measurements [4,15,16], and scanning- tunneling microscopy [17,18], no clear-cut conclusion could be drawn about the phase structures. This is due to the fact that, on the one hand, x-ray powder spectra show a smooth dependence of the interlayer distances across the observed sequences of phases [11,19] and, on the other hand, x-ray plates obtained from oriented samples do not allow one to discriminate the different structures [19]. Thus, only indirect experiments, such as dielectric [7,20,21] and electro-optical [5] measurements, or conoscopic figure observations [4,22,23] could establish unequivocally the ferro-, antiferro-, or ferrielectric nature of the reported phases. However, these data do not give any insight about the molecular steps of reorganization from one structure to another. In this respect, the phenomenological model proposed by Orihara and Ishibashi [24] does not discuss the *mechanisms* that may lead to a ferrielectric ordering.

The aim of the present work is to show that the whole set of experimental data concerning these phases can be understood in terms of an *azimuthal reorientation of the molecular subunits,* assuming a *bilayer* periodicity for the smectic stacking. Besides, we give a detailed description of the *inhomogeneous* structures of the ferroelectric, antiferroelectric, and ferrielectric phases, which were not considered in the *homogeneous* model of Ref. [24].

The paper is organized as follows. In Sec. II a theoretical description is given of the possible dipolar configurations that may arise in bilayer antiferroelectric and ferrielectric smectics. Section III contains a discussion of the theoretical predictions of our model and of the available experimental data reported for antiferroelectric and ferrielectric liquid crystals.

II. THEORETICAL MODEL

A. Homogeneous case

Let us assume a bilayer stacking of dipolar molecules and introduce for its phenomenological description the two axial vectors η_1 and η_2, defined as follows:

$$\begin{aligned}\eta_1&=(-n_{1y}n_{1z},n_{1x}n_{1z})\\ \eta_2&=(-n_{2y}n_{2z},n_{2x}n_{2z})\ ,\end{aligned}\tag{1}$$

where the n_{iu} $(i=1,2;\ u=x,y,z)$ are the components of the director in the ith layer, and the space variables (x,y) and z indicate, respectively, the in-plane coordinates and the direction perpendicular to the layers. The four components of η_1 and η_2 span a four-dimensional reducible representation of the space group $G_0=D_\infty\otimes T_Z$, which is associated with the parent chiral Sm-A phase. This representation decomposes in two irreducible representations of G_0 that are respectively spanned by the planar vectors

$$\eta_P=\eta_1+\eta_2,\eta_A=\eta_1-\eta_2\ .\tag{2}$$

η_P and η_A transform, respectively, as the in-layer *polarization* $P=\mathbf{p}_1+\mathbf{p}_2$ *and antipolarization* $\mathbf{A}=\mathbf{p}_1-\mathbf{p}_2$, where $\mathbf{p}_1$ and $\mathbf{p}_2$ are the polarizations of two adjacent layers. One can note that under the symmetry operations of G_0, η_P and η_A can be distinguished only by the translations $t_Z\in T_Z$, as $t_Z(\eta_P)=\eta_P$ and $t_Z(\eta_A)=-\eta_A$.

Using the symmetry properties of η_P and η_A, one can construct the order-parameter expansion associated with the observed sequences of phase transitions. It is formed by three basis invariants (rational basis of integrity [25]),

 ©1994 The American Physical Society

which are

$$I_1=\eta_P{}^2,\quad I_2=\eta_A{}^2,\quad I_3=(\boldsymbol{\eta}_P\cdot\boldsymbol{\eta}_A)^2=\eta_P{}^2\eta_A^2\cos^2\alpha\ , \tag{3}$$

where α is the angle between $\boldsymbol{\eta}_P$ and $\boldsymbol{\eta}_A$ in real space as well as in the order-parameter space. The corresponding order-parameter expansion can thus be written under the more general form

$$\Phi_H=(\alpha/2)I_1+(a/2)I_2+cI_1I_2+dI_3+\cdots\ . \tag{4}$$

Standard methods of minimization of Φ_H [25] yield *five ordered low-symmetry phases,* which are defined by the following equilibrium values of the order parameter $(\boldsymbol{\eta}_P,\boldsymbol{\eta}_A)$:

I. $|\boldsymbol{\eta}_P|\neq 0,\ |\boldsymbol{\eta}_A|=0$;

II. $|\boldsymbol{\eta}_P|=0,\ |\boldsymbol{\eta}_A|\neq 0$;

III. $|\boldsymbol{\eta}_P|\neq|\boldsymbol{\eta}_A|\neq 0$ and $\boldsymbol{\eta}_P\|\boldsymbol{\eta}_A\ (\alpha=0)$;

IV. $|\boldsymbol{\eta}_P|\neq|\boldsymbol{\eta}_A|\neq 0$ and $\boldsymbol{\eta}_P\perp\boldsymbol{\eta}_A\ (\alpha=\pi)$;

V. $|\boldsymbol{\eta}_P|\neq|\boldsymbol{\eta}_A|\neq 0$ and $0<\alpha<\pi$.

The smectic ordering corresponding to the preceding equilibrium values of the order parameter are represented in Fig. 1. One can see that three types of dipolar orders may be found. Figure 1(a) coincides with a *ferroelectric monolayer* ordering with dipoles remaining parallel from one layer to the other. Figure 1(b) corresponds to an *antiferroelectric bilayer* ordering, with an antiparallel orientation for adjacent dipoles. Figures 1(c)–1(e) represent the three types of *ferrielectric* ordering, which can be distinguished by their tilt *and* azimuthal angles. Thus, phase III is a ferrielectric structure in which two adjacent layers possess a distinct tilt angle and opposed azimuthal angles for the molecules. In the structure shown in Fig. 1(d) the molecular subunits possess the same tilt angles but distinct arbitrary azimuthal angles. At last, the ferrielectric ordering represented in Fig. 1(e) is characterized by distinct tilt *and* azimuthal angles for the molecules.

In Fig. 2 is represented a section of the phase diagram that exhibits the domain of stability of the five above-mentioned phases *far from the smectic-A phase* in the plane of the phenomenological coefficients $(d,\alpha-a)$. One can see that the phases are separated by second-order transition lines and that two four-phase points can be found at which merge the phases (I, III, IV, V) and (III, II, IV, V), respectively. One can note also that the lower symmetry phase (V) may possess a broad range of stability and that, depending on the actual thermodynamic path, various sequences of ferrielectric and antiferroelectric phases can be expected.

In this section, only a homogeneous form, given by Eq. (4), of the thermodynamic potential was discussed. It does not take into account the influence of the chiral symmetry of the molecules, i.e., the *helicoïdal incommensurate character* of the structure along the z axis. We will now discuss a more realistic model that accounts for the inhomogeneous properties of the phases.

B. Inhomogeneous case

When considering the chiral symmetry of the Sm-A parent phase, the following invariants must be added to the thermodynamic potential. These were not taken explicitly into account in the calculations by Ishibashi and Orihara [24]:

$$I_4=\left[\frac{\partial\boldsymbol{\eta}_p}{\partial z}\right]^2,\quad I_5=\left[\frac{\partial\boldsymbol{\eta}_A}{\partial z}\right]^2,$$

$$I_6=\eta_{py}\frac{\partial\eta_{px}}{\partial z}-\eta_{px}\frac{\partial\eta_{py}}{\partial z}\ , \tag{5}$$

$$I_7=\eta_{Ay}\frac{\partial\eta_{Ax}}{\partial z}-\eta_{Ax}\frac{\partial\eta_{Ay}}{\partial z}\ .$$

We will now introduce the main assumption of our model, namely, that the *transition mechanism between the various phases corresponds essentially to an azimuthal reorientation of the molecular subunits.* This mechanism, which assumes that the tilt angles remain largely unchanged across the phases, will be shown, in Sec. III to be *in reasonable agreement with the available experimental*

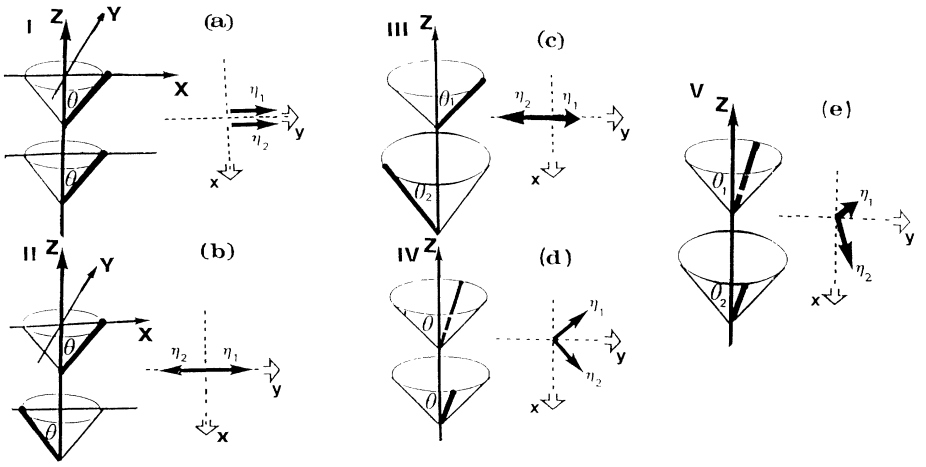

FIG. 1. Smectic structures corresponding to a bilayer ordering. (a) ferroelectric phase I; (b) antiferroelectric phase II; (c), (d), and (e) ferrielectric phases denoted III, IV, and V in the text. One elementary unit cell is represented. On the right-hand side of each figure the vectors $\boldsymbol{\eta}_1$ and $\boldsymbol{\eta}_2$ characterizing the tilts in adjacent layers are given in the $(x$-$y)$ plane.

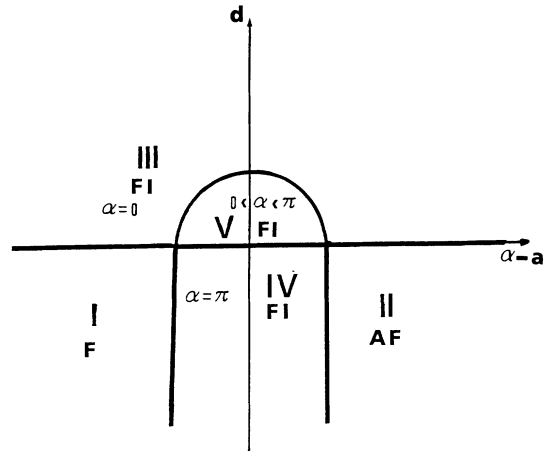

FIG. 2. Theoretical phase diagram associated with the potential Φ_H, given by Eq. (4), in the plane of the phenomenological coefficients $(d,\alpha-a)$. The figure represents a section of the diagram showing the domain of stability of the five polar smectic phases, far from the domain of stability of the parent Sm-A phase. The transition lines are all of second order, as only the lowest degree of Φ_H, which involves the full set of stable phases, is taken into account. The diagram is constructed following the method described in Ref. [25].

data.

One can introduce formally this *conical approximation* (i.e., the molecules can turn freely on *cones* possessing fixed vertex angles) by using the auxiliary variables

$$\phi=(\phi_i+\phi_{i+1})/2, \quad \psi=(\phi_i-\phi_{i+1})/2 , \tag{6}$$

where ϕ_i is the azimuthal angle of the ith layer, measured with respect to the x axis. ϕ has the meaning of the azimuthal angle of the polarization within a bilayer, whereas ψ is the angle of the polarization between the two antiferroelectric sublattices. Thus the form of the order parameter within the ith layer can be written as

$$\eta_{P_i}=(\eta_{P_0}\cos\phi_i,\eta_{P_0}\sin\phi_i) \tag{7}$$

where, as the result of the conical approximation, *the amplitude η_{P_0} is assumed to be constant.* Accordingly, the mean value of the order parameter within a layer can be written

$$\begin{aligned}\eta_P&=2\eta_{P_0}(\cos\phi\cos\psi,\sin\phi\cos\psi) ,\\ \eta_A&=2\eta_{P_0}(-\sin\phi\sin\psi,\sin\psi\cos\phi) ,\end{aligned} \tag{8}$$

and the invariants (3) and (5) become

$$\begin{aligned}&I_1=4\eta_{p0}^2\cos^2\psi, \quad I_2=4\eta_{p0}^2\sin^2\psi, \quad I_3=0 ,\\ &I_4=4\eta_{p0}^2\left[\left[\frac{\partial\phi}{\partial z}\right]^2\cos^2\psi+\left[\frac{\partial\psi}{\partial z}\right]^2\sin^2\psi\right] ,\\ &I_5=4\eta_{p0}^2\left[\left[\frac{\partial\phi}{\partial z}\right]^2\sin^2\psi+\left[\frac{\partial\psi}{\partial z}\right]^2\cos^2\psi\right] ,\\ &I_6=-4\eta_{p0}^2\left[\frac{\partial\phi}{\partial z}\right]\cos^2\psi , \quad I_7=-4\eta_{p0}^2\left[\frac{\partial\phi}{\partial z}\right]\sin^2\psi .\end{aligned} \tag{9}$$

The Landau-Ginzburg energy of the inhomogeneous system can thus be written

$$F=\int\left[\frac{\alpha}{2}I_1+\frac{\beta}{4}I_1^2+\frac{a}{2}I_2+\frac{b}{4}I_2^2+cI_1I_2+\frac{g_1}{2}I_4+\frac{g_2}{2}I_5-\lambda_1I_6-\lambda_2I_7\right]dz , \tag{10}$$

where the sum runs over the thickness of the sample. In (10) the terms containing the invariants I_1 and I_2 are restricted to the fourth degree in the order-parameter components. Including η_{P_0} in the phenomenological coefficients, one can rewrite F under the more easily handled form

$$\begin{aligned}F=\int\Bigg[&\frac{1}{2}\left[\frac{\partial\phi}{\partial z}\right]^2(g^++g^-\cos2\psi)\\&+\frac{1}{2}\left[\frac{\partial\psi}{\partial z}\right]^2(g^+-g^-\cos2\psi)\\&-\left[\frac{\partial\phi}{\partial z}\right](\lambda^++\lambda^-\cos2\psi)\\&+\frac{a_1}{2}\cos2\psi+\frac{b_1}{4}\cos^22\psi\Bigg]dz ,\end{aligned} \tag{11}$$

where $g^+=(g_1+g_2)/2$, $g^-=(g_1-g_2)/2$, $\lambda^+=(\lambda_1+\lambda_2)/2$, $\lambda^-=(\lambda_1-\lambda_2)/2$, $a_1=\alpha/2-a/2+\beta/4-b/4$, and $b_1=\beta/4+b/4-c/4$.

The equations of state expressing the minimization of F, as given by Eq. (11), using the Euler-Lagrange variational procedure, are

$$\begin{aligned}&\frac{\partial\phi}{\partial z}(g^++g^-\cos2\psi)-(\lambda^++\lambda^-\cos2\psi)=C ,\\ &\frac{\partial^2\phi}{\partial z^2}(g^+-g^-\cos2\psi)+\left[\frac{\partial\psi}{\partial z}\right]^2g^-\sin2\psi\\ &\quad=\Bigg[\left[\frac{\partial\phi}{\partial z}\right]^2g^-\sin2\psi+2\frac{\partial\phi}{\partial z}\lambda^-\sin2\psi-a_1\sin2\psi\\ &\qquad-b_1\sin2\psi\cos2\psi\Bigg] ,\end{aligned} \tag{12}$$

where C is the first integral value that depends on the external parameters. It is easy to show that the only stable solution of (12) corresponding to a helicoidal structure is

$$\phi=kz, \quad \psi=C_0 , \tag{13}$$

where $\mathbf{k}$ is the wave vector of the helix and C_0 is a constant; k and C_0 do not depend on z but vary in function of the external variables. In other words, one obtained an *in-phase azimuthal angle* ϕ that depends linearly on z, whereas the *azimuthal antiphase angle* ψ is *independent* of the z variable. This simplifying result can be interpreted as the fact that a *single wave vector determines the helicoïdal structure of the bilayer phases,* i.e., when mov-

ing along z, the angle between the polarization vectors associated with the two sublattices *remains fixed,* and thus the two helices associated with η_P and η_A, *are dependent on one another* and *turn in phase.*

From Eqs. (12) and (13) one can deduce that three possible stable helicoïdal structures can be obtained, depending on the values of the phenomenological coefficients: a *ferroelectric* helicoïdal structure for $\psi=0$, an *antiferroelectric* helicoïdal structure for $\psi=\pi/2$, and a *ferrielectric* helicoïdal structure for $\pi/2>\psi>0$. The possible phase diagrams corresponding to different values of the phenomenological coefficients are shown in Fig. 3. The main features of these diagrams have been obtained from exact calculation using a procedure given in the Appendix. The various diagrams shown in Fig. 3 are distinguished by the number

$$B=\lambda^- g^+ - g^- \lambda^+ , \tag{14}$$

which characterizes the chirality of bilayer smectic structures.

In order to represent the phase diagrams in the concentration temperature (x-T) plane, where $x=(n_R-n_L)/\{2(n_R+n_L)\}$ is the ratio of right-to-left handed molecules, let us define the following linear transformation:

$$\begin{aligned} &\lambda_1=\lambda_{10}x, \quad \lambda_2=\lambda_{20}x, \quad B=B_0 x , \\ &A=-a_1 g^- + b_1 g^+ + (\lambda^-)^2 \\ &\quad = A_0(T-T_0)+(\lambda_0^-)^2 x^2 , \end{aligned} \tag{15}$$

where T_0 is a reference temperature and λ_{10}, λ_{20}, B_0, and A_0 are constants. One can note here that for a nonracemic mixture characterized by $x\neq 0$, the operation $x\rightarrow -x$ is a symmetry operation leaving unchanged the properties of the sample *except the sign of the helix.* The Lifshitz invariant changes sign under this transformation, whereas the other invariants in F remain unchanged. The linear transformation given by Eq. (15) is the simplest transformation that fulfills the condition that the diagram must be symmetric with respect to $x=0$.

In Fig. 3 one can see that the ferrielectric structure is always located *between* the ferro- and antiferroelectric structures. Besides, the diagram contains lines of second- *and first-* order transitions that merge at three phase points and also tricritical points.

In summary, the more remarkable result obtained from the bilayer model presented in this section is that, for the first time, a *ferrielectric helicoidal phase* is shown to be stable in liquid-crystal systems and to possess the following specific features. *Its helical pitch is modified by the antiphase azimuthal angle* ψ, due to the coupling between the wave vector k and ψ. As ψ does not depend on the space variable z but depends on concentration and temperature, the pitch of the ferrielectric helix will consequently be dependent on these external variables. This intrinsic property does not require any phenomenological assumption, and especially higher degree terms are not needed, as in the theory of ferroelectric liquid crystals [26]. Besides, the temperature dependence of the helical pitch is monotonic, and Fig. 4 shows the $k(T)$ dependence for various concentrations in the sequence of ordered phases.

III. DISCUSSION OF THE MODEL AND COMPARISON TO EXPERIMENTS

Let us now analyze the experimental data obtained on antiferroelectric liquid crystals in light of our theoretical model. As noted in the Introduction the whole set of experimental results reported up to now does not allow a clear-cut structural determination of the phases. Depending on the two configurations found in Sec. II for the ferrielectric phase, two possible mechanisms associated with the transition between ordered phases can be proposed, which imply different experimental behaviors.

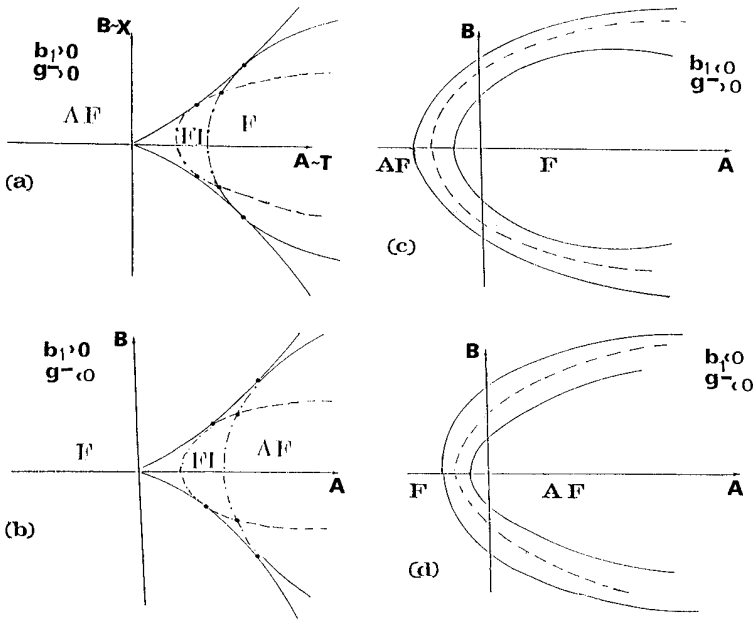

FIG. 3. Phase diagrams associated with the Landau-Ginzburg potential F given by Eq. (11), assuming a helicoïdal stable solution, and different values of the phenomenological coefficients g^- and b_1. The diagrams are worked out following a procedure described in the Appendix. The B and A coefficients are defined by Eqs. (14) and (15) and are proportional to concentration and temperature, respectively. Full lines are limit-of-stability lines and dashed lines are first-order transition lines. In (a) and (b), dotted-dashed lines represent second-order transition lines.

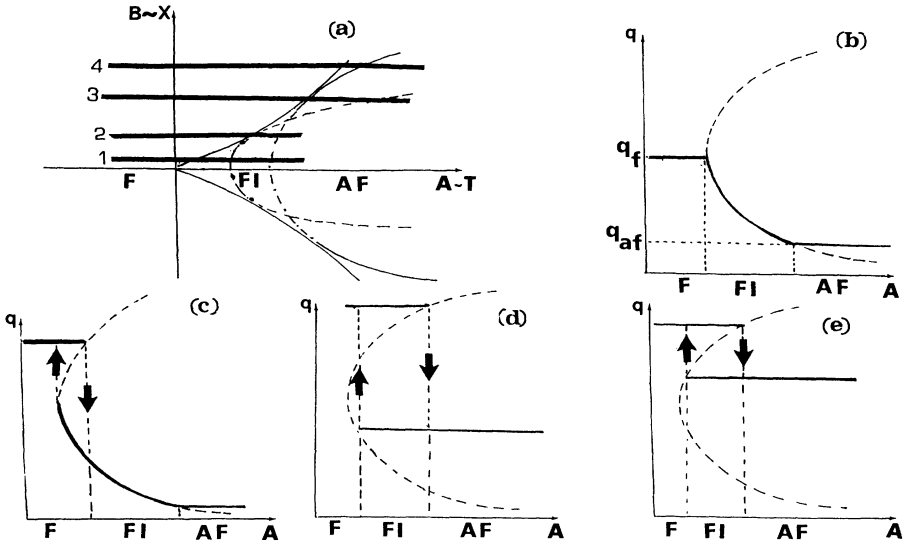

FIG. 4. Temperature dependence of the k vector associated with the azimuthal angle ϕ of the polarization for four different thermodynamic paths corresponding to different values of the concentration x. Figures (b), (c), (d), and (e) correspond, respectively, to the paths denoted (1), (2), (3), and (4) in Fig. (a). For path (1) one has two antiferro-ferri and ferri-ferro *second-order transitions.* For path (2) the ferri-ferro transition becomes first order. For path (3) the ferrielectric phase is metastable within the domain of coexistence of the antiferro and ferro phases. For path (4) the ferri phase is unstable.

If the ferro-antiferro transition takes place through phase III, with a restanding up of the molecules located in one layer, while the molecules of the adjacent layer remain practically unchanged or even more inclined [Fig. 1(c)], then one should observe, on the one hand, a nonmonotonic dependence of the interlayer distance as a function of temperature when going across the sequence of ferro-ferri-antiferro transitions. On the other hand, such a mechanism would result in a modulation of the electronic density along the z axis, displaying a bilayered periodicity that should be observed in x-ray experiments. Furthermore, a drastic change of the average tilt angle with temperature should be detected through electroclinic effect measurements.

The ferro-antiferro transitions through phase IV [Fig. 1(d)] yield opposite experimental consequences, as the transition mechanism is an azimuthal reorientation of the directors of two adjacent layers in two opposite directions, the molecules being inclined by the *same* tilt angle θ. In this case a *smooth* dependence of the interlayer distance should be observed, as well as the absence of any detectable modulation along the z axis, as the tilt is identical from one layer to another. Actually, as the structure factor in x-ray diffraction is proportional to the square of $\sin\theta_i$, where θ_i is the tilt angle in the ith layer, phase IV should not be distinguishable in x-ray diffraction observations when going from the ferroelectric phase I or the antiferroelectric phase II. Here the electroclinic effect should only reveal a very weak temperature dependence of the tilt.

Let us compare the preceding alternative predictions, as deduced from our model, with the available data reported for optically pure MHPOBC. The temperature dependence of the layer spacing $d(T)$ in function of temperature has been measured by Suzuki *et al.* [11] who found, by means of small-angle x-ray diffraction, a very slow dependence of $d(T)$ when crossing C^*, $C\gamma^*$, and $C_A{}^*$. The chevron structure found in the ordered phases of MHPOBC [27] above 65 °C shows also a weak asymptoticlike dependence of the in-layer tilt angle δ within the sm-C^*, Sm-$C_\gamma{}^*$, and Sm-$C_A{}^*$ phases. The electroclinic effect measured by Hiraoka *et al.* [28] reveals that the apparent tilt angle as a function of the applied electric field in the *three* phases displays nearly identical plateaus and tilt angles, a fact that also favors a very slight tilt dependence on temperature.

The preceding facts are thus compatible with an *antiphase* orientation of the subunits in two neighboring layers, as assumed in our model, and do not confirm the alternative mechanism that assumes a temperature dependence for θ. No traces of modulation with a double or multilayer periodicity were found in small-angle x-ray experiments on oriented samples, which reveal very similar diffractograms for the three C^*, $C_\gamma{}^*$, and $C_A{}^*$ smectic phases [11,12,19]. This result can be interpreted in the framework of our model of the ferro-ferri-antiferro sequence of phases, in connection with the fact that the smectic layers are well pronounced in the three phases, as attested by the observation of third harmonics of the electronic density in x-ray spectra. Let us emphasize here that in the *three*-layer model of the Sm-$C_\gamma{}^*$ phase proposed by Takezoe *et al.* [29], which is schematized in Fig. 5(a), the molecules are assumed to possess the same values for the tilt angle in three successive layers. Such a situation implies the additional restriction $\theta_1=\theta_2$, as the symmetry of the system imposes only two equal angles among three successive tilt angles. This condition can be realized only at one concentration and at one temperature in the phase diagram, and thus the corresponding ordering should be unobservable experimentally. The configuration represented in Fig. 5(b) has the same symmetry as that assumed in the Takezoe *et al.* [29] model, but it would imply a temperature dependence of the tilt angle that has not been observed experimentally.

The discussion of the possible structural configuration of the Sm-$C_\gamma{}^*$ phase should also take into account the conoscopic figures observed under applied electric field that were found on thick homeotropic cells of MHPOBC [4,22]. These figures reveal a number of features, namely (1) a modification under applied field that is attributed to

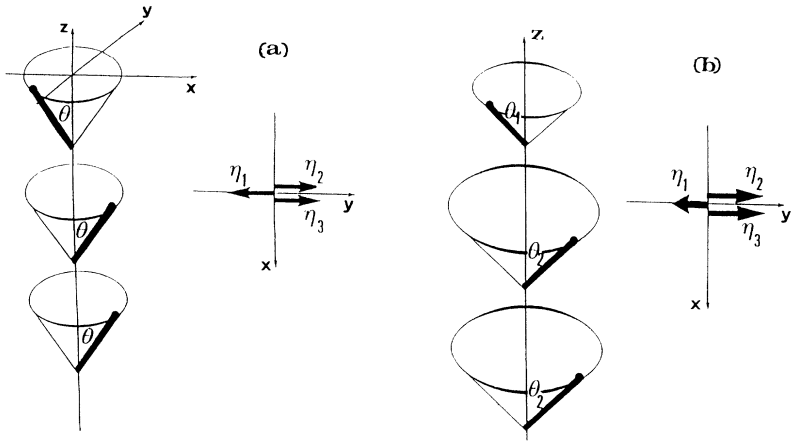

FIG. 5. (a) One among the possible three-layer configurations assumed in the model of Takazoe *et al.* [29] for the ferrielectric structure, using the same notation as in Fig. 1(b). General configuration for a three-layer model, without any specific assumption on the tilt angles.

a strong dielectric anisotropy, (2) the fact that in the Sm-C_γ^* phases the optical plane is parallel to the field direction in the region of low fields and becomes, for larger fields, perpendicular to the field direction. This latter fact was used as an argument against the bilayer model. However, one can show that a strong dielectric anisotropy should also allow a similar behavior in the framework of a *bilayer* model [30].

Let us finally analyze the contribution to the dielectric susceptibility and optical response of the azimuthal antiphase mode, which in our model is the primary degree of freedom, in the considered sequence of phases. In order to investigate this contribution, we assume that the coupling between the so-called Goldstone mode ϕ and the azimuthal antiphase mode ψ is weak. Accordingly the helicity of the phases has a weak influence on the ψ mode, and one can write the part of the free energy that depends on ψ under the simplified form

$$\tilde{\Phi}_H \sim \tfrac{1}{2}a_1 \cos 2\psi + \tfrac{1}{4}b_1 \cos^2 2\psi \ . \tag{16}$$

The phase diagram corresponding to Eq. (16) is shown in Fig. 6(a) in the plane (a_1, b_1). The dielectric susceptibility $\chi = \partial P/\partial E$ can be deduced from the field-dependent potential $\tilde{\Phi} = \tilde{\Phi}_H - \mathbf{E}\cdot\mathbf{P} = \tilde{\Phi}_H - EP_0 \cos\psi$. One finds the more general form

$$\chi \approx \frac{\sin^2\psi}{\dfrac{\partial^2\tilde{\Phi}_H}{\partial\psi^2} - \operatorname{cotan}\psi \dfrac{\partial\tilde{\Phi}_H}{\partial\psi}} \ , \tag{17}$$

which yields in the ferro- (F), antiferro- (AF), and ferrielectric (FI) phases

$$\chi_F \approx 0, \quad \chi_{AF} \approx \frac{1}{2(a_1 - b_1)}, \quad \chi_{FI} \approx \frac{1}{-4(a_1 - b_1)} \ . \tag{18}$$

The temperature dependence of χ across the three phases is shown in Fig. 6(b). One can see that the contribution of the azimuthal antiphase mode to the susceptibility *diverges* through the second-order ferri-antiferro transition and *reaches its minimum* at the ferro-ferri transition. In fact, the phases are always helicoïdal, and the Goldstone mode is thus present when the local polarization is different from zero. However, the contribution of the Goldstone mode to χ is proportional to the polarization, decreases in the ferrielectric phase and vanishes at the ferri-antiferro transition. Consequently the contribution of the ψ mode to χ should become the most impor-

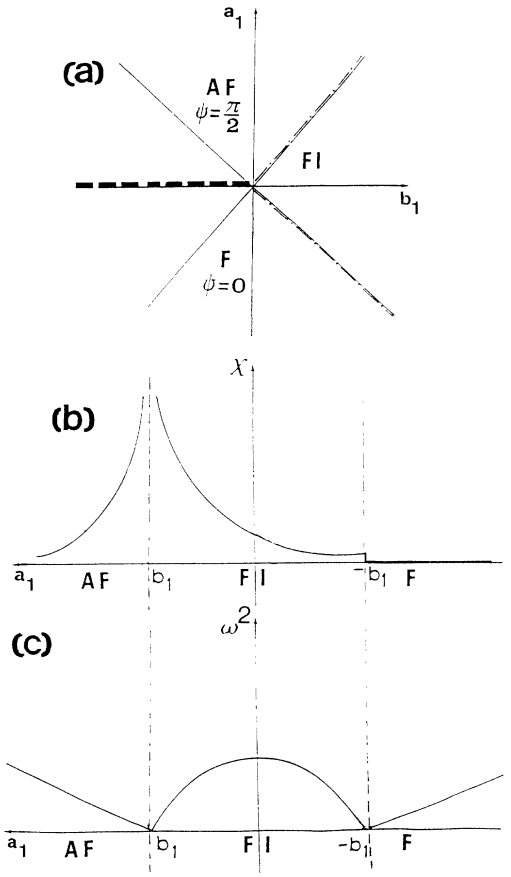

FIG. 6. (a) Schematic phase diagram associated with the homogeneous potential $\Phi_H(\psi)$ given by Eq. (16), in the plane of the phenomenological coefficients (a_1, b_1). Full, dashed, and dashed-dotted lines are, respectively, stability lines and lines of first- and second-order transitions. (b) Temperature dependence of the contribution of the azimuthal antiphase mode ψ, to the dielectric susceptibility χ, following Eq. (18). (c) Temperature dependence of the square of the frequency of the azimuthal antiphase mode ψ in optical response following Eq. (19).

tant in the vicinity of the ferri-antiferro transition.

Figure 6(c) shows the contribution of the azimuthal mode to the optical response, which is proportional to the square of the frequency in optical measurements $\omega^2 \sim \partial^2 \tilde{\Phi}_H / \partial \psi^2$. One finds that

$$\begin{aligned} &\omega_F^2 \sim -2(a_1+b_1) , \\ &\omega_{\mathrm{AF}}^2 \sim 2(a_1-b_1) , \\ &\omega_{\mathrm{FI}}^2 \sim 2(b_1^2-a_1^2)/b_1 . \end{aligned} \tag{19}$$

Thus, in contrast with the dielectric response, the optical response to the azimuthal mode is identical for the ferro-ferri and ferri-antiferro transitions. Besides, from the microscopic point of view, the contribution of the azimuthal mode ψ to the dielectric susceptibility should be observed in dielectric measurements *at very low frequencies.* This is due, on the one hand, to the general property that the order of energy of the azimuthal rotation and the corresponding relaxation frequencies are small in liquid-crystal systems and on the other hand, that in contrast to usual ferroelectric liquid-crystal phases in which the relaxation frequency of the azimuthal Goldstone mode is high due to the helix deformation, here the homogeneous character of the azimuthal antiphase mode ψ should involve actually low energy and low frequency.

Concerning the applicability of the theoretical phase diagrams presented in Figs. 3(a) and 3(b), it can be noted that they differ from the experimental temperature-concentration diagrams in the fact that the ferrielectric phase appears experimentally in the vicinity of optically pure substances [2,3,31], and that the ferri-ferri and antiferro-ferri transitions are reported to be first order [8,11,13]. In the framework of our model, such features can be obtained by considering six-degree terms in $\tilde{\Phi}_H$. In this case, it is easy to show that the second-order transition lines in Fig. 3, would transform into first-order transition lines, and that the ferrielectric phase will appear *far* from the racemic mixture line $x=0$, in the vicinity of the pure substance at $x=\pm\frac{1}{2}$.

As a final remark, let us emphasize that the homogeneous potential Φ_H given by Eq. (4) used in our model is associated with a *four-dimensional* representation of the symmetry group of the smectic-A phase, but depends only on the *three* variables $|\eta_P|$, $|\eta_A|$, and α and the fourth variable remaining free. Accordingly in dynamical spectra one should observe in the more general case *three normal modes,* and only *one Goldstone mode,* and not only two normal modes as pointed out by Zeks, Blinc, and Copic [32].

APPENDIX

In this appendix we describe the procedure that allows us to work out the phase diagrams of Fig. 3. When substituting the stable solutions (13) in the Landau-Ginzburg potential (11), one gets by integrating with respect to the z variable,

$$\begin{aligned} F(k,\psi) = &(k^2/2)(g^+ + g^- \cos 2\psi) \\ &- k((\lambda^+ + \lambda^-)\cos 2\psi) + (a_1/2)\cos 2\psi \\ &+ (b_1/2)\cos^2 2\psi . \end{aligned} \tag{A1}$$

The phase diagram associated with $F(k,\psi)$ is the bifurcation diagram corresponding to the family of functions $F(k,\psi)$ with the six parameters g^+, g^-, λ^+, λ^-, a_1, and b_1. The corresponding equations of state are

$$\begin{aligned} &\frac{\partial F}{\partial k} = k(g^+ + g^- \cos 2\psi) - (\lambda^+ + \lambda^- \cos 2\psi) = 0 , \\ &\frac{\partial F}{\partial \psi} = \sin 2\psi (2k\lambda^+ - k^2 g^- - a_1 - b_1 \cos 2\psi) = 0 . \end{aligned} \tag{A2}$$

The ferroelectric phase corresponds to the equilibrium conditions ($\sin 2\psi = 0$, $\cos 2\psi = 1$) and to the stability condition

$$a_1 \le -b_1 + 2\lambda^- \left[\frac{\lambda^+ + \lambda^-}{g^+ + g^-} \right] - g^- \left[\frac{\lambda^+ + \lambda^-}{g^+ + g^-} \right]^2 . \tag{A3}$$

The antiferroelectric phase is given by the equilibrium conditions ($\sin 2\psi = 0$, $\cos 2\psi = -1$) and the stability condition

$$a_1 \ge b_1 + 2\lambda^- \left[\frac{\lambda^+ - \lambda^-}{g^+ - g^-} \right] - g^- \left[\frac{\lambda^+ - \lambda^-}{g^+ - g^-} \right]^2 . \tag{A4}$$

For the ferrielectric phase one has $\sin 2\psi \neq 0$ and

$$2k\lambda^+ - k^2 g^- - a_1 - b_1 \cos 2\psi = 0 . \tag{A5}$$

The region of stability of this latter phase is limited by *three* curves: the so-called *discriminant curve,* or line of stability with respect to *homophase* fluctuations [25,33], and two other curves that represent the stability lines with respect to *heterophase* fluctuations of the ferro-ferri and antiferro-ferri phase transition [25,33]. These two lines are given by Eq. (A2) and by the limit of stability condition

$$\frac{\partial^2 F}{\partial \psi^2} \frac{\partial^2 F}{\partial k^2} - \left[\frac{\partial^2 F}{\partial k \, \partial \psi} \right]^2 = 0 ,$$

which can be written

$$2 \sin^2 2\psi [b_1 (g^+ + g^- \cos 2\psi) - 2(\lambda^- - k g^-)^2] = 0 . \tag{A6}$$

The discriminant curve coincides with Eq. (A6), which can be solved by changing the variables in order to locate the most degenerate singularity at the origin [33]. The relevant change in variables is here

$$\begin{aligned} &q = \lambda^- - g^- k , \\ &A = -a_1 g^- + b_1 g^+ + (\lambda^-)^2 , \\ &B = \lambda^- g^+ - g^- \lambda^+ . \end{aligned} \tag{A7}$$

Consequently, one gets the boundary of stability lines under the simple parametric form

$$A q - b_1 B - q^3 = 0, \quad b_1 B - 2q^3 = 0 , \tag{A8}$$

and the discriminant curve is given by

$$4A^3-27b_1^2B^2=0\ , \tag{A9}$$

which are semicubic parabolas represented in Fig. 3. The stability curves with respect to heterophase fluctuations can be written using the same change in variables (A7). One gets

$$A=b_1(g^+ +g^-)+B^2/(g^+ +g^-)^2 \tag{A10}$$

for the ferroelectric phase boundary line and

$$A=b_1(g^+ -g^-)+B^2/(g^+ -g^-)^2 \tag{A11}$$

for the antiferroelectric phase boundary line. The corresponding parabolas coincide with an equality in Eqs. (A3) and (A4) and are *second-order transition lines.* The *first-order transition line* between the ferro- and antiferroelectric phases is given by the condition $F_{\text{ferro}}=F_{\text{antiferro}}$. It has the form

$$A=b_1g^+ +B^2/\{(g^+ -g^-)(g^+ +g^-)\}\ . \tag{A12}$$

The coordinates of the specific points of the phase diagrams in Fig. 3 can also be calculated algebraically, as, for example, the point of intersection of the first-order ferro-antiferro transition line with the ferro-ferri second-order transition line. It is given by

$$\begin{aligned} A&=(b_1/2)(3g^+ +g^-)\ , \\ B_{1,2}&=\pm(b_1/2)(g^+ \pm g^-)^{1/2}(g^+ +g^-)\ . \end{aligned} \tag{A13}$$

One can note that the phase diagrams of Fig. 3 are symmetric with respect to the line $B=0$. The B parameter reflects the inhomogeneous part of the Ginzburg-Landau potential and characterizes phenomenologically the *chirality* of the bilayer smectric phases under consideration.

[1] A. D. L. Chandani, E. Gorecka, Y. Ouchi, H. Takezoe, and A. Fukuda, Jpn. J. Appl. Phys. **28**, L1265 (1989).

[2] M. Fukui, H. Orihara, Y. Yamada, N. Yamamoto, and Y. Ishibashi, Jpn. J. Appl. Phys. **28**, L849 (1989).

[3] H. Takezoe, J. Lee, A. D. L. Chandani, E. Gorecka, Y. Ouchi, A. Fukuda, K. Terashima, and K. Furukawa, Ferroelectrics **114**, 187 (1991).

[4] E. Gorecka, A. D. L. Chandani, Y. Ouchi, H. Takezoe, and A. Fukuda, Jpn. J. Appl. Phys. **29**, 131 (1990).

[5] J. Lee, A. D. L. Chandani, K. Itoh, Y. Ouchi, H. Takezoe, and A. Fukuda, Jpn. J. Appl. Phys. **29**, 1122 (1990).

[6] J. Lee, Y. Ouchi, H. Takezoe, A. Fukuda, and J. Watanabe, J. Phys. Cond. Matter **2**, SA271 (1990).

[7] K. Hiraoka, T. Tagushi, Y. Ouchi, H. Takezoe, and A. Fukuda, Jpn. J. Appl. Phys. **29**, L103 (1990).

[8] A. D. L. Chandani, Y. Ouchi, H. Takezoe, A. Fukuda, K. Terashima, K. Furukawa, and A. Kishi, Jpn. J. Appl. Phys. **28**, L1261 (1989).

[9] K. Furukawa, K. Terashima, M. Ichibachi, S. Saitoh, K. Miyazawa, and T. Inukai, Ferroelectrics **85**, 451 (1988).

[10] T. Isozaki, Y. Suzuki, I. Kawamura, M. Mori, N. Yamamoto, Y. Yamada, H. Orihara, and Y. Ishibashi, Jpn. J. Appl. Phys. **30**, L1573 (1991).

[11] A. Suzuki, H. Orihara, Y. Ishibashi, Y. Yamada, N. Yamamoto, K. Mori, K. Nakamura, Y. Suzuki, T. Hagiwara, Y. Kawamura, and M. Fukui, Jpn. J. Appl. Phys. **29**, L336 (1990).

[12] M. Johno, Y. Ouchi, H. Takezoe, and A. Fukuda, Jpn. J. Appl. Phys. **29**, L111 (1990).

[13] S. Inui, S. Kawano, M. Saito, H. Iwane, Y. Takanishi, K. Hiraoka, Y. Ouchi, H. Takezoe, and A. Fukuda, Jpn. J. Appl. Phys. **29** L987 (1990).

[14] H. Orihara, T. Fujikawa, Y. Ishibashi, Y. Yamada, N. Yamamoto, K. Mori, K. Nakamura, Y. Suzuki, T. Hagiwara, and I. Kawamura, Jpn. J. Appl. Phys. **29**, L333 (1990).

[15] Y. Takanishi, K. Hiraoka, V. K. Agrawal, H. Takezoe, A. Fukada, and M. Matsushita, Jpn. J. Appl. Phys. **30**, 2023 (1991).

[16] J. Lee, Y. Ouchi, H. Takezoe, A. Fukada, and J. Watanabe, J. Phys. Cond. Matter **2**, L103 (1990).

[17] H. Takezoe, A. Fukada, A. Ikeda, Y. Takanishi, J. Umemoto, J. Watanabe, H. Iwane, M. Hara, and K. Itoh, Ferroelectrics **122**, 167 (1991).

[18] M. Hara, T. Umemoto, H. Takezoe, A. F. Garito, and H. Sasabe, Jpn. J. Appl. Phys. **30**, L2052 (1991).

[19] A. M. Levelut and P. Gisse (private communication).

[20] M. Fukui, H. Orihara, A. Suzuki, Y. Ishibashi, Y. Yamada, N. Yamamoto, K. Nakamura, Y. Suzuki, and I. Kawamura, Jpn. J. Appl. Phys. **29**, L329 (1990).

[21] K. Hiraoka, A. D. L. Chandani, E. Gorecka, Y. Ouchi, H. Takezoe, and A. Fukuda, Jpn. J. Appl. Phys. **29**, L1473 (1990).

[22] N. Okabe, Y. Suzuki, I. Kawamura, I. Isozaki, H. Takezoe, and A. Fukado, Jpn. J. Appl. Phys. **31**, L793 (1992).

[23] T. Isozaki, K. Hiraoka, Y. Takanishi, H. Fukuda, Y. Suzuki, and I. Kawamura, Liquid Crystals **12**, 59 (1992).

[24] H. Orihara and Y. Ishibashi, Jpn. J. Appl. Phys. **29**, L115 (1990).

[25] Yu. M. Gufan, *Structural Phase Transitions* (Nauka, Moscow, 1982); J. C. Tolédano and P. Tolédano, *The Landau Theory of Phase Transitions* (World Scientific, Singapore, 1987), Chap. 2.

[26] R. Blinc, B. Zeks, M. Copic, A. Levstik, I. Musevic, and I. Drevensek, Ferroelectrics **104**, 159 (1990).

[27] M. Johno, A. D. L. Chandani, Y. Ouchi, H. Takezoe, A. Fukuda, M. Ichibashi, and K. Furukawa, Jpn. J. Appl. Phys. **30**, L1819 (1991).

[28] K. Hiraoka, Y. Takanishi, K. Skarp, H. Takezoe, and F. Fukuda, Jpn. J. Appl. Phys. **30**, L1819 (1991) .

[29] H. Takezoe, J. Lee, Y. Ouchi, and A. Fukuda, Mol. Cryst. Liq. Cryst. **202**, 85 (1991).

[30] A. A. Bulbitch, V. L. Lorman, and P. Tolédano (unpublished).

[31] T. Isozaki, T. Fujikawa, H. Takezoe, A. Fukuda, J. Hagiwara, Y. Suzuki, and I. Kawamura, Jpn. J. Appl. Phys. **31**, L1453 (1992).

[32] B. Zeks, R. Blinc, and M. Copic, Ferroelectrics **122**, 221 (1991).

[33] Y. Kutyin, V. L. Lorman, and S. V. Pavlov, Sov. Phys. Usp. **34**, 497 (1991).